Real-Gas Flowfields about Three-Dimensional Configurations

A. Balakrishnan*
PEDA Corporation, Palo Alto, California
W.C. Davy†
NASA Ames Research Center, Moffett Field, California
and
C.K. Lombard‡
PEDA Corporation, Palo Alto, California

Real-gas, inviscid supersonic flowfields over a three-dimensional configuration are determined using a factored implicit algorithm. Air in chemical equilibrium is considered and its local thermodynamic properties are computed by an equilibrium composition method. Numerical solutions are presented for both real and ideal gases at three different Mach numbers and at two different altitudes. Selected results are illustrated by contour plots and are also tabulated for future reference. The results obtained compare well with existing tabulated numerical solutions and hence validate the solution technique.

Nomenclature

a = sound speed
A = Jacobian matrix, defined by Eqs. (15) and (16)
B = Jacobian matrix, defined by Eq. (15)
C = Jacobian matrix, defined by Eq. (15)
e = total energy density
E = flux vector, defined by Eq. (2)
F = flux vector, defined by Eq. (2)
G = flux vector, defined by Eq. (2)
h = static enthalpy; also parameter used to select the spatial order of the numerical scheme in Eq. (14)
i = internal energy
I = identity matrix
J = Jacobian of the coordinate transformation, defined by Eq. (6)
ℓ = length
M = molecular weight of the mixture; also Mach number
p = nondimensional pressure
q = conservative variable vector
R = normalized radial distance
T = normalized temperature, defined by Eq. (3)
u = velocity component in the x coordinate direction
v = velocity component in the y coordinate direction; also dimensional characteristic velocity
w = velocity component in the z coordinate direction
x,y,z = Cartesian coordinate directions
Z = compressibility, defined by Eq. (12)
α = angle of attack
β = ratio of static enthalpy to internal energy
γ = isentropic exponent
δ = central difference operator; also shock standoff distance
Δ, ∇ = forward and backward difference operators
ϵ = artificial dissipation smoothing parameter
ζ = coordinate in the circumferential direction
η = coordinate in the normal direction
θ = parameter defined by Eq. (18)
ξ = coordinate in the axial direction
ρ = gas mixture density
τ = nondimensional time
ϕ = parameter defined by Eq. (17)

Subscripts

e = explicit
i = implicit
N = nose
ref = reference
t = time derivative
∞ = freestream

Superscripts

n = nth time step
$(\ )^*$ = dimensional quantity
$(\hat{\ })$ = scaled by Jacobian

Presented as Paper 83-0581 at the AIAA 21st Aerospace Sciences Meeting, Reno, Nev., Jan. 10-13, 1983; received March 7, 1984; revision received July 20, 1984.

*Engineer. Member AIAA.
†Research Scientist. Member AIAA.
‡President. Member AIAA.

Introduction

ACCURATE knowledge of heating environments of current and advanced space transportation systems (STS), such as the Space Shuttle Orbiter and the aeroassisted orbital transfer vehicle (AOTV), is essential to the thermal protection system design of these vehicles. Entry conditions for these vehicles are usually severe, with speeds of several kilometers per second resulting in shock temperatures of thousands of Kelvin. In addition to the large entry velocities, the planetary atmosphere may consist of a radiatively participating medium. Shock-layer gases that envelope these classes of vehicles may or may not be chemically equilibrated. For design purposes, one has to consider all of the physical processes, including chemistry, diffusion, and radiation. Experimental simulation of these entry conditions is very difficult, if not impossible, in ground-based facilities and is very expensive. Thus, it is essential to numerically simulate these entry environments with sophisticated computer codes. However, computer codes that treat arbitrary three-dimensional configurations (including real-gas effects and radiation transfer) have not been developed due to computer speed and memory limitations. In fact, only in the last few

years have computational fluid dynamicists[1,2] developed practical numerical algorithms for three-dimensional problems, although limited to ideal gases. With the availability of high-speed, large-memory computers, such as the CRAY 1S, and with the recent advances in computational fluid dynamics and aerothermodynamics, it is now possible to numerically simulate the full complexity of entry environments of hypersonic vehicles.

In a recent paper,[3] Howe identified the aerothermodynamic problems to be addressed during conceptual design studies of advanced STS. For these systems, he outlined long- and near-term efforts that must be undertaken concurrently; as part of long-term efforts, three-dimensional real-gas flowfield codes must be developed that include the effects of mass, momentum, energy, species transport, and gaseous radiative transfer under equilibrium and nonequilibrium conditions. In a similar context, Park[4] emphasized the need for multidimensional flowfield calculations with chemistry and chemical kinetics.

The present paper is a first step in fulfilling the needs described in Refs. 3 and 4. This paper describes the modifications to include equilibrium chemistry to an already existing three-dimensional ideal-gas code developed by Kutler et al.[5] The analysis presented here is general in that any reacting gas mixture can be treated. It follows closely the work reported by Davy et al.[6] for two-dimensional and axisymmetric configurations. This work differs from earlier work reported in the literature mainly in the way the thermodynamic properties of the gas mixture are obtained. To date, most of real-gas flowfield computations were performed using tabulated thermodynamic properties along with a table look-up or interpolation routines followed by ex post facto computation of species distribution, if these were required. This approach, although relatively fast, is of limited generality since change in the gas elemental composition requires construction of new thermodynamic tables. In this work, the chemical equilibrium relations are solved at each computational node point, yielding thermodynamic properties and species equilibrium compositions. Although increasing computational time, this approach eliminates the errors associated with table look-up schemes and is completely general so that it is easily extended to include wall blowing of ablation products, chemical kinetics, and radiative transfer.

A brief literature survey is included in the next section, followed by the governing equations, numerical method, and boundary conditions. To validate the numerical method, calculations are performed for ideal and equilibrium air at Mach numbers of 10, 15 and 20, and the results obtained are compared with the tabulated data of Lyubimov and Rusanov.[7] Effects of real gas on the flowfield are discussed in detail.

Literature Survey

Some of the earlier work by various researchers in computing real-gas flowfields are briefly summarized in this section. Lomax and Iouye[8] used an inverse method (i.e., predicting the body shape for the assumed shock shape) to obtain solutions for inviscid perfect and equlibrium airflows over a sphere, ellipsoids, and paraboloids. Using equilibrium air thermodynamic properties tabulated as functions of two state properties such as pressure and density or pressure and entropy, they estimated such thermodynamic properties as sound speed, enthalpy, and temperature by interpolation. These quantities were then used to predict the shock standoff distance and the flowfield between the body and shock. Comparison of shock shapes and sonic lines between real- and ideal-gas solutions showed significant differences.

Lyubimov and Rusanov[9] thoroughly investigated the inviscid flow past blunt bodies and reported their analysis and results in two parts. Reference 9 contains the method of calculating three-dimensional unsteady flows past such blunt bodies as a sphere, paraboloid, ellipsoid, hyperboloid, and blunted cone. Also, the analyses of plane, axisymmetric, and three-dimensional real-gas flows were included. Reference 7 contains detailed tables of flowfield and chemistry variables for the above-mentioned configurations at several Mach numbers. The accuracy of the tables is discussed in detail in Ref. 7; according to the authors, the computed results were determined to be reliable up to four decimal places. In addition to the two Cartesian velocity components u and v for axisymmetric flows, Lyubimov and Rusanov used pressure and density as the other two independent gasdynamic variables. In their real-gas flow analysis, they used pressure and density as state-defining variables and obtained sound speed, enthalpy, and temperature from the Tchebycheff polynomial fits of these properties for equilibrium air. This approach was followed in order to reduce the computational time.

Kutler et al.,[10] using the property table for equilibrium air assembled in Ref. 8, obtained inviscid flowfield solutions around the three-dimensional Space Shuttle Orbiter. Marconi et al.[11] solved the steady three-dimensional Euler equations including real-gas effects and obtained flowfield solutions about complex geometries using curve fits of Mollier charts. Li,[12] using analytical curve fits for equilibrium air due to Tannehill et al.,[13] obtained viscous real-gas flowfield around the Space Shuttle for a freestream Mach number of 22 at an angle of attack of 40 deg. Lewis and coworkers[14,15] have considered the effect of real-gas on the three-dimensional viscous flowfield where the equilibrium air properties were again obtained from a property table. Utilizing the computer code developed in Ref. 11, Maus et al.[16] studied the effect of real gas on the Space Shuttle aerodynamics. Real-gas effects were found to increase the axial force coefficient, particularly at high Mach numbers and at high-entry-altitude conditions. Also they found that the effect of real gas was to decrease the normal force coefficient. It was estimated that the net effect of real gas was a shift in the center of pressure, thus contributing significant changes in the aerodynamics of the Shuttle. Davy et al.[6] successfully coupled the gasdynamic governing equations with chemistry and obtained a solution at peak heating for the Galileo probe entry into the Jovian atmosphere. They discovered that for computational stability the chemistry variables should be evaluated at constant pressure and enthalpy conditions. This sequence of coupling the gasdynamic and chemistry variables is adopted in the present work.

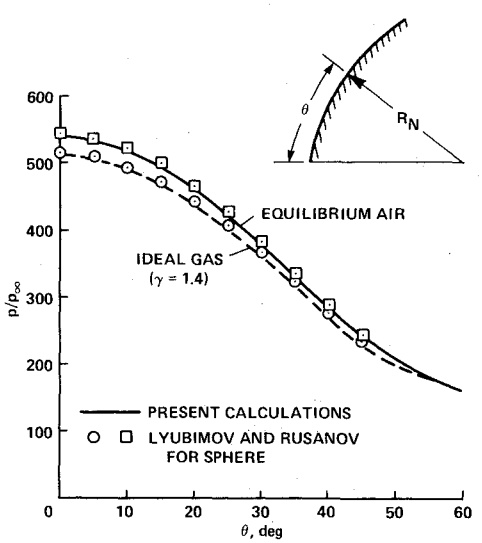

Fig. 1 Comparison of surface pressure distribution for an ideal gas and equilibrium air with the calculated results of Ref. 7, $M_\infty = 20$, $H = 50$ km.

Governing Equations

Starting with the unsteady three-dimensional Navier-Stokes equations in Cartesian coordinates, the governing equations for an inviscid, nonconducting fluid are obtained in arbitrary curvilinear ξ, η, ζ, τ coordinates and in strong conservation law form. The transformed equations can be written in nondimensional form as

$$\frac{\partial \hat{q}}{\partial \tau}+\frac{\partial \hat{E}}{\partial \xi}+\frac{\partial \hat{F}}{\partial \eta}+\frac{\partial \hat{G}}{\partial \zeta}=0 \tag{1}$$

where

$$\hat{q}=\frac{1}{J}\begin{bmatrix}\rho\\ \rho u\\ \rho v\\ \rho w\\ e\end{bmatrix},\ \hat{E}=\frac{1}{J}\begin{bmatrix}\rho U\\ \rho uU+\xi_x p\\ \rho vU+\xi_y p\\ \rho wU+\xi_z p\\ (e+p)U-\xi_t p\end{bmatrix} \tag{2}$$

$$\hat{F}=\frac{1}{J}\begin{bmatrix}\rho V\\ \rho uV+\eta_x p\\ \rho vV+\eta_y p\\ \rho wV+\eta_z p\\ (e+p)V-\eta_t p\end{bmatrix},\ \hat{G}=\frac{1}{J}\begin{bmatrix}\rho W\\ \rho uW+\zeta_x p\\ \rho vW+\zeta_y p\\ \rho wW+\zeta_z p\\ (e+p)W-\zeta_t p\end{bmatrix}$$

and the contravariant velocities U, V, and W are given by

$$\begin{aligned}U&=\xi_t+u\xi_x+v\xi_y+w\xi_z\\ V&=\eta_t+u\eta_x+v\eta_y+w\eta_z\\ W&=\zeta_t+u\zeta_x+v\zeta_y+w\zeta_z\end{aligned} \tag{3}$$

The Cartesian velocity components u, v, and w are nondimensionalized by a dimensional characteristic velocity v^*, defined as

$$v^*=\sqrt{\frac{p_\infty}{\rho_\infty}}=\frac{a_\infty}{\sqrt{\gamma_\infty}} \tag{4}$$

where p_∞, ρ_∞, a_∞, and γ_∞ are the freestream pressure, density, sound speed, and isentropic exponent, respectively. The pressure and density that appear in Eq. (2) are scaled by the corresponding freestream quantities. All lengths are nondimensionalized by a reference length ℓ_{ref}. Time is referenced to a characteristic time (ℓ_{ref}/v^*) and total energy density e is scaled by $\rho_\infty v^{*2}$.

The metric terms that appear in Eqs. (2) and (3) are defined by

$$\begin{aligned}\xi_x&=J(y_\eta z_\zeta-y_\zeta z_\eta), & \eta_x&=J(y_\zeta z_\xi-y_\xi z_\zeta)\\ \xi_y&=J(z_\eta x_\zeta-z_\zeta x_\eta), & \eta_y&=J(z_\zeta x_\xi-z_\xi x_\zeta)\\ \xi_z&=J(x_\eta y_\zeta-x_\zeta y_\eta), & \eta_z&=J(x_\zeta y_\xi-x_\xi y_\zeta)\\ \zeta_x&=J(y_\xi z_\eta-y_\eta z_\xi), & \xi_t&=-x_\tau\xi_x-y_\tau\xi_y-z_\tau\xi_z\\ \zeta_y&=J(z_\xi x_\eta-z_\eta x_\xi), & \eta_t&=-x_\tau\eta_x-y_\tau\eta_y-z_\tau\eta_z\\ \zeta_z&=J(x_\xi y_\eta-x_\eta\zeta_\xi), & \zeta_t&=-x_\tau\zeta_x-y_\tau\zeta_y-z_\tau\xi_z\end{aligned} \tag{5}$$

where J is the Jacobian of the transformation and is given by

$$J^{-1}=x_\xi(y_\eta z_\zeta-y_\zeta z_\eta)+x_\eta(y_\zeta z_\xi-y_\xi z_\zeta)+x_\zeta(y_\xi z_\eta-z_\xi y_\eta) \tag{6}$$

The relationship that remains to be established is between the pressure and total energy density e. From the definition of static enthalpy h and internal energy i, one gets

$$h=i+p/\rho \tag{7}$$

Introducing a parameter β as the ratio of static enthalpy to internal energy, Eq. (7) can be written as

$$i=p/(\beta-1)\rho \tag{8}$$

The total energy density can be written as the sum of the internal energy and kinetic energy, i.e.,

$$e/\rho=i+0.5(u^2+v^2+w^2) \tag{9}$$

Combining Eqs. (8) and (9), a relation for the pressure and total energy density e is obtained, i.e.,

$$p=(\beta-1)[e-0.5\rho(u^2+v^2+w^2)] \tag{10}$$

Equation (10) is general for any gas or gas mixture. The quantity β is a variable property that depends on the heat of formation and equilibrium species composition. For an ideal gas, this quantity is the familiar ratio of specific heats γ. The quantity β plays an important role in real-gas flowfield computations; Davy et al.[6] give a thorough discussion of β in their paper.

Another relationship that is useful for computational purposes is the nondimensional equation of state, i.e.,

$$p=\rho ZT \tag{11}$$

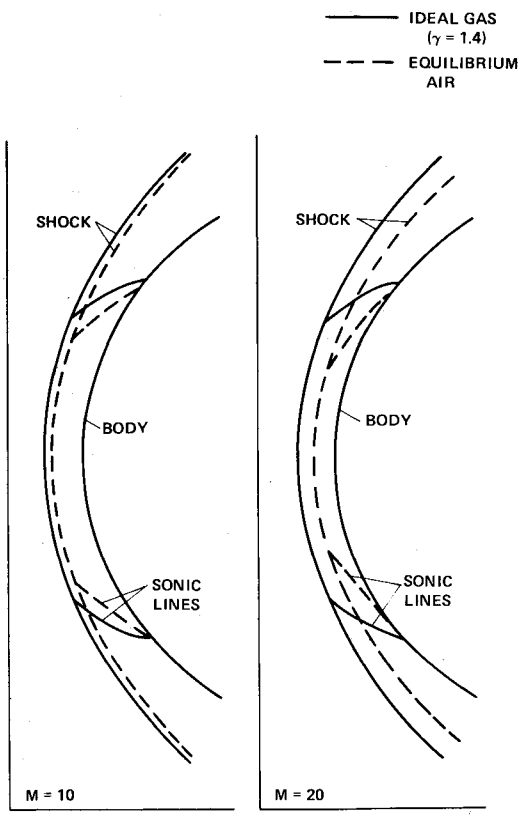

Fig. 2 Effect of Mach number and real gas ($H=20$ km) on the shock standoff distance and sonic line.

where the compressibility Z is given by

$$Z=M_\infty/M \tag{12}$$

Combining Eqs. (8), (10), and (11), one obtains for non-dimensional temperature T

$$T=\frac{(\beta-1)}{Z}\left[\frac{e}{\rho}-0.5(u^2+v^2+w^2)\right] \tag{13}$$

Until now, the thermodynamic quantities that appear in Eqs. (10-13) are not restricted to any gas or gas mixture. Also, we have not specified how these quantities will be evaluated. The primary difference between the present approach and those mentioned previously is the way these thermodynamic quantities are computed. An equilibrium composition method due to Gordon and McBride[17] is used here rather than the conventional table look-up schemes employed in Refs. 7-14.

Numerical Method

The finite difference scheme used to solve the governing equations is the implicit, approximate factorization algorithm in delta form due to Beam and Warming.[2] This particular procedure is widely used and has been successfully applied by Pulliam and Steger[18] and Kutler et al.[5] for three-dimenisional viscous flows. Detailed description of the method and derivation are given in Refs. 2 and 18. For inviscid flow the governing equations take the following form after time linearization of the component vectors $\hat{E}$, $\hat{F}$, and $\hat{G}$ and applying the Beam and Warming algorithm:

$$\begin{aligned}
&(I+h\delta_\xi\hat{A}^n-\epsilon_i J^{-1}\nabla_\xi\Delta_\xi J)\Delta\hat{q}^n_{\cdot\cdot}=\Delta\tau[\delta_\xi\hat{E}^n+\delta_\eta\hat{F}^n\\
&\quad+\delta_\zeta\hat{G}^n]-\epsilon_e J^{-1}[(\nabla_\xi\Delta_\xi)^2+(\nabla_\eta\Delta_\eta)^2+(\nabla_\zeta\Delta_\zeta)^2]J\hat{q}^n\\
&(I+h\delta_\eta\hat{B}^n-\epsilon_i J^{-1}\nabla_\eta\Delta_\eta J)\Delta\hat{q}^n_{\cdot\cdot}=\Delta\hat{q}^n_{\cdot\cdot}\\
&(I+h\delta_\zeta\hat{C}^n-\epsilon_i J^{-1}\nabla_\zeta\Delta_\zeta J)\Delta\hat{q}^n=\Delta\hat{q}^n_{\cdot\cdot}
\end{aligned} \tag{14}$$

where I is the identity matrix and the Jacobian matrices $\hat{A}$, $\hat{B}$, and $\hat{C}$ are defined as

$$\hat{A}=\frac{\partial\hat{E}}{\partial\hat{q}},\quad \hat{B}=\frac{\partial\hat{F}}{\partial\hat{q}},\quad \hat{C}=\frac{\partial\hat{G}}{\partial\hat{q}} \tag{15}$$

and the δ are the central difference operators, Δ and ∇ are the forward and backward difference operators, and ϵ_i and ϵ_e are the implicit second-order and the explicit fourth-order smoothing parameters, respectively. The Jacobian matrices $\hat{A}$, $\hat{B}$, and $\hat{C}$ differ from those given in Ref. 18 due tothe introduction of the real-gas parameter β. The real-gas Jacobian matrix $\hat{A}$ is

$$\hat{A}=\begin{bmatrix}
\xi_t & \xi_x & \xi_y & \xi_z & 0\\
\xi_x\phi-u\theta & \xi_t+\theta-(\beta-2)u\xi_x & \xi_y u-(\beta-1)v\xi_x & \xi_z u-(\beta-1)w\xi_x & \xi_x(\beta-1)\\
\xi_y\phi-v\theta & \xi_x v-(\beta-1)u\xi_y & \xi_t+\theta-(\beta-2)v\xi_y & \xi_z v-(\beta-1)w\xi_y & \xi_y(\beta-1)\\
\xi_z\phi-w\theta & \xi_x w-(\beta-1)u\xi_z & \xi_y w-(\beta-1)v\xi_z & \xi_t+\theta-(\beta-2)w\xi_z & \xi_z(\beta-1)\\
\theta\left[2\phi-\beta\frac{e}{\rho}\right] & \xi_x\left(\beta\frac{e}{\rho}-\phi\right)-(\beta-1)u\theta & \xi_y\left(\beta\frac{e}{\rho}-\phi\right)-(\beta-1)v\theta & \xi_z\left(\beta\frac{e}{\rho}-\phi\right)-(\beta-1)w\theta & \xi_t+\beta\theta
\end{bmatrix} \tag{16}$$

where

$$\phi=0.5(\beta-1)(u^2+v^2+w^2) \tag{17}$$

and

$$\theta=\xi_x u+\xi_y v+\xi_z w \tag{18}$$

The Jacobian matrices $\hat{B}$ and $\hat{C}$ are obtained by substituting the appropriate metrics defined in Eq. (5). The thermodynamic quantity β that appears in the above equations and the equilibrium composition of species are obtained by iteratively solving the nonlinear species equilibrium coefficient equations, see Gordon and McBride.[17] As the solution converges following a short starting transient, changes in conditions at a given computational node are small enough so that the chemistry scheme converges quickly, usually in two or three iterations. The equilibrium state of a gas mixture is defined by two state variables. The Gordon and McBride method allows the use of either pressure and enthalpy or pressure and temperature for state definition. From the state definition, composition and hence all relevant thermodynamic properties of the gas mixture are computed.

Boundary Conditions

The wall boundary condition procedure is explained in detail in Ref. 5 and is adopted here without modification. Briefly, the inviscid tangency condition along with an adiabatic wall condition are used to obtain the three components of velocity and density. To obtain the pressure at the body surface, a normal momentum equation, formed by combining the three transformed momentum equations, is integrated. At the shock boundary, the flow variables downstream of the shock are determined using a shock-fitting approach described in Ref. 5. However, the approach has been modified to include real-gas effects. For example, the density behind the shock is obtained from the Rankine-Hugoniot relation for a real gas. At the outflow boundary, a simple linear extrapolation of the conservative variables is employed. As described in Ref. 5, at the coordinate singularity, local averaging is done for the flowfield variables. The coupling between the gasdynamic and chemistry variables is done as follows. For a specified value of pressure and enthalpy, compressibility Z, the quantity β, and the chemical composition of the gas mixture are computed. These variables are used along with the equation of state to find the density and internal energy. Then, as a part of the solution technique, the three velocity components are updated by assuming that the mass fluxes are conserved. With the use of density and the velocity components, energy density, and hence pressure, are updated.

Results

To validate the real-gas computer code and to show the effect of real gas on the flowfield, seven cases are considered: three ideal-gas solutions at Mach numbers 10, 15, and 20, three equilibrium air solutions at the above Mach numbers at an entry altitude of 20 km, and a solution at Mach number of 20 at an entry altitude of 50 km. For ideal-gas computations, a constant value of isentropic constant γ of 1.4 is used. For equilibrium air computations, the freestream composition of air is approximated to be $N_2=0.7885$ and $O_2=0.2115$, by volume. The trace species argon and CO_2 are neglected. For calculation purposes, the following species set is used: O_2, N_2, O, N, NO, e, O^-, O^+, N^-, N^+, and NO^+. For the above species, the most recent JANAF data[19] for specific heat at constant pressure are fit with approximating functions.

The flowfield around the nose cap section, defined here as the first 0.38 m from the stagnation point of the Space Shuttle Orbiter, is considered. The Space Shuttle geometry was constructed using the analytic approximations given in Ref. 10. In modeling the Shuttle geometry, for the first 45 deg from the axis, a spherical segment assumption is used. After the 45 deg line, the Shuttle geometry slowly deviates from a sphere. All the computations were performed for zero angle of attack. These restrictions on the flow and on the geometry are imposed so that the results can be compared with those available in Ref. 7. Even though these restrictions reduce the problem to a two-dimensional axisymmetric flow around an approximately spherical segment, the computations were all performed using the three-dimensional code. The computational grid consisted of 13 nodes in the axial (ξ) direction, 17 nodes in the normal (η) direction, and 21 nodes in the circumferential (ζ) direction. The procedure described in Ref. 5 is used to initialize the flowfield.

For inviscid flow simulation, severe gradients in the normal direction will not develop because the diffusive mechanisms are not modeled. So the uniform spacing of 0.0625 is considered to be adequate for the computations performed in this work. Grid clustering is not required; indeed, it will only increase the computer resources needed to obtain a converged solution. The convergence criteria employed for the finite difference solution are as follows. The root mean square and maximum shock speeds as well as the residuals of the gasdynamic variables were monitored at each iteration. The solution is deemed converged when these three errors have been reduced to less than 10^{-3}. In addition, the local total enthalpy was compared with the freestream total enthalpy to insure energy conservation. The chemistry iteration was considered converged if the change in mole fractions of all species was below a preselected tolerance value, 10^{-5} in this case.

As noted in the numerical method section, ϵ_i and ϵ_e are the implicit and explicit numerical dissipation parameters. Pulliam and Steger[18] give a thorough discussion of their importance and their effect on the stability of the numerical scheme. Following the recommendations of Ref. 18, in the present computations ϵ_e is equal to $\Delta\tau$. Then ϵ_i is set equal to $2\epsilon_e$. Note that $\Delta\tau$ varies with Courant number. When the Courant number can be increased following the subsidence of initial transients, which are probably because of the introduction of chemistry terms to a perfect-gas solution, the relative magnitude of the added artificial dissipation remains constant. In the present computations, the maximum $\Delta\tau$ reached was 10^{-3}-10^{-2}.

To validate the computer code, the ideal-gas solutions are first obtained. Comparing these results with Ref. 7, excellent agreement is found for all gas dynamic variables. The ideal-gas solutions are then used to start the real-gas solutions. Figure 1 compares the surface pressure distribution around the body, in the symmetry plane, for both an ideal gas and equilibrium air at a Mach number of 20 and an entry altitude of 50 km with the tabulated data of Ref. 7. As shown, good agreement is obtained. Note the strong influence of real gas on the surface pressure, particularly in the subsonic region of the flowfield. For comparison purposes, only data up to the 45 deg line are shown since the geometry used in the present computations deviates from a true sphere beyond that point.

Real-gas effects on the shock shape and sonic line are illustrated in Fig. 2 for free-stream Mach numbers of 10 and 20 and an entry altitude of 20 km. Real-gas influences the shock standoff only slightly at a Mach number of 10; however, at Mach 20, there is a significant reduction in the shock-layer thickness. This figure illustrates the general notion that real gases reduce the shock-layer thickness and move the sonic line toward the stagnation line. Accurate prediction of shock-layer thickness is important for radiating shock-layer gases, since it significantly influences the radiative flux to the wall. Also, accurate prediction of the sonic line location is important as the solution generated by the time-dependent three-dimensional code forms the initial plane or starting point from which a parabolized Navier-Stokes (PNS) space-marching procedure will initiate. For flows at large angles of attack, the windward sonic line moves far downstream on the body. Thus, for solving large angle-of-attack problems, one is then forced to include a large part of the forebody for generating a starting solution for the PNS codes. With the inclusion of the real-gas effects, this problem is somewhat alleviated.

To further illustrate the combined effect of Mach number and real gas on the flowfield, the gas dynamic variables ρ/ρ_∞, T (in Kelvin), and the normalized shock standoff distance, δ/R_N, are summarized in Table 1, at the wall and at the shock. As can be inferred from Table 1, density, temperature, and shock standoff distances are strongly influenced by chemistry, particularly at high Mach numbers. For example, for an ideal gas, as Mach number is increased, the density ratio approaches a constant value close to 6 at the shock. However, for equilibrium air, as the Mach number is increased, the density ratio greatly increases. At high Mach numbers, the shock temperature for a real gas is significantly lower than that for an ideal gas. For instance, at a Mach number of 20 and at entry altitude of 20 km, the real-gas shock temperature is less than half that for an ideal gas. However, at a Mach number of 10, the real-gas influence on the shock temperature is not as strong; the real-gas shock temperature is only about 20% lower than the ideal-gas shock temperature. As mentioned before, real-gas effects significantly influence the shock-layer thickness. Specifically, the normal shock standoff distance is reduced by as much as 45% from the ideal-gas value at a Mach number of 20 and an entry altitude of 20 km.

The last two rows of Table 1 serve to illustrate the effect of altitude on the real-gas flowfield. For the same freestream Mach number of 20, the density ratio at the shock is larger for a higher entry altitude, since the decreased freestream density causes a shift in the equilibrium composition that results in a higher density ratio. The strong shock jump conditions have an effect on the shock-layer temperature and on the shock standoff distance. At the normal shock (0 deg), the effect of higher altitude is to decrease the shock-layer temperature by about 1000 K. Also, the standoff distance decreases as the altitude increases.

The chemistry variables are compared in Table 2 with the tabulated data of Ref. 7. Data are included along the stagnation (0 deg) line in Table 2a and 45 deg line in Table 2b. In the tables, selected chemistry variables are presented at the wall ($\eta=0$), at $\eta=0.25$, 0.50, and at the shock ($\eta=1.0$). Excellent agreement is obtained for equilibrium compositions of O, N_2, N, and NO. The temperatures agree within 1%. The entropies differ by roughly a constant value of 0.25 cal/g·K.

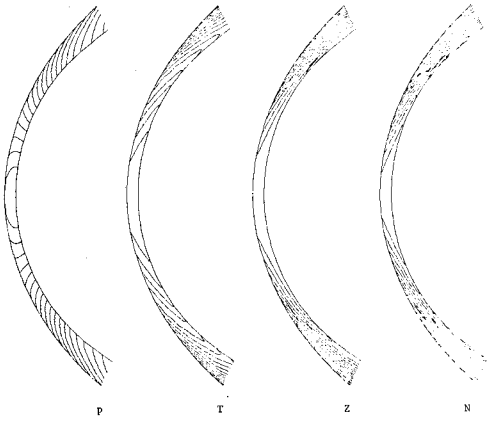

Fig. 3 Contour plots of gasdynamic and chemistry variables for equilibrium air at $M_\infty = 20$, $H = 50$ km.

Table 1 Effect of real gas and Mach number on gas dynamic variables at the body and at the shock $\theta = 0°$ (along stagnation line)

Mach number	Altitude, km	At the wall p/p_∞ Ideal gas ($\gamma = 1.4$)	p/p_∞ Equi. air	ρ/ρ_∞ Ideal gas	ρ/ρ_∞ Equi. air	$T(K)$ Ideal gas	$T(K)$ Equi. air	At the shock p/p_∞ Ideal gas	p/p_∞ Equi. air	ρ/ρ_∞ Ideal gas	ρ/ρ_∞ Equi. air	$T(K)$ Ideal gas	$T(K)$ Equi. air	δ/R_N Ideal gas	δ/R_N Equi. air
10	20	129	131	6.14	8.00	4552	3444	117	122	5.71	7.54	4417	3402	0.141	0.112
15	20	290	300	6.29	10.06	9968	5468	262	282	5.87	9.67	9683	5367	0.137	0.086
20	20	513	531	6.35	11.77	17492	7334	467	509	5.93	11.36	17055	7295	0.135	0.076
20	50	513	540	6.35	15.17	17492	6386	467	521	5.93	14.72	17055	6364	0.135	0.060

Table 2 Comparison of results for equilibrium air ($M_\infty = 20$, $H = 20$ km)

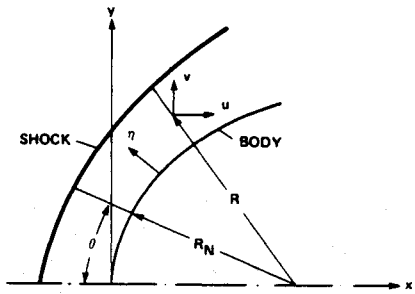

EQUILIBRIUM AIR M_∞ = 20, H = 20 km

Variable	Normalized distance from wall, η: 0.0 Present	0.0 Ref. 7	0.25 Present	0.25 Ref. 7	0.50 Present	0.50 Ref. 7	0.75 Present	0.75 Ref. 7	1.0 Present	1.0 Ref. 7
Species mole fraction										
O_2	1.027-3	9.265-4	1.020-3	9.233-4	1.025-3	9.232-4	1.031-3	9.232-4	1.034-3	9.232-4
O	2.941-1	2.933-1	2.940-1	2.927-1	2.941-1	2.928-1	2.944-1	2.930-1	2.948-1	2.933-1
N_2	4.774-1	4.776-1	4.765-1	4.776-1	4.775-1	4.780-1	4.789-1	4.787-1	4.807-1	4.801-1
N	2.061-1	2.003-1	2.072-1	2.000-1	2.060-1	1.996-1	2.043-1	1.987-1	2.021-1	1.970-1
NO	2.054-2	2.070-2	2.046-2	2.066-2	2.050-2	2.065-2	2.054-2	2.062-2	2.054-2	2.057-2
e	4.105-4	3.945-4	4.125-4	3.935-4	4.099-4	3.921-4	4.059-4	3.891-4	4.003-4	3.840-4
Normalized sound speed c	7.249	7.269	7.253	7.268	7.247	7.264	7.236	7.256	7.221	7.243
Temp. (K) T	7334	7395	7339	7394	7331	7388	7317	7377	7295	7357
Static enthalpy h (cal/gm)	4217	4212	4226	4210	4216	4205	4200	4195	4179	4179
Entropy s (cal/gm K)	2.553	2.794	2.554	2.793	2.554	2.793	2.553	2.793	2.554	2.794

a) $\theta = 0$ deg (along stagnation line)

Species mole fraction										
O_2	1.064-3	9.563-4	1.327-3	1.205-3	1.818-3	1.685-3	2.955-3	2.747-3	6.002-3	6.595-3
O	3.046-1	3.033-1	3.065-1	3.047-1	3.080-1	3.061-1	3.076-1	3.056-1	3.001-1	2.959-1
N_2	5.231-1	5.205-1	5.419-1	5.394-1	5.651-1	5.631-1	5.932-1	5.898-1	6.224-1	6.198-1
N	1.512-1	1.487-1	1.282-1	1.251-1	9.978-2	9.600-2	6.557-2	6.321-2	3.045-2	2.736-2
NO	1.947-2	1.942-2	2.158-2	2.158-2	2.484-2	2.498-2	3.039-2	3.048-2	4.094-2	4.209-2
e	2.729-4	2.516-4	2.376-4	2.154-4	1.923-4	1.700-4	1.348-4	1.172-4	7.483-5	5.534-5
Normalized sound speed c	6.831	6.859	6.735	6.759	6.609	6.627	6.436	6.456	6.222	6.187
Temp. (K) T	6725	6780	6608	6656	6438	6473	6171	6202	5772	5715
Static enthalpy h (cal/gm)	3679	3695	3501	3513	3274	3282	2983	3003	2613	2623
Entropy s (cal/gm K)	2.581	2.799	2.557	2.769	2.527	2.730	2.490	2.682	2.448	2.612

b) $\theta = 45$ deg

Table 3 Gasdynamic variables for flow of an ideal gas around a sphere at $M_\infty = 15$ and $\alpha = 0$ deg.

θ	Variable	Normalized distance from wall, η									Variable
		0.000	0.125	0.250	0.375	0.500	0.625	0.750	0.875	1.000	
0	R	0.1000 1	0.1017 1	0.1034 1	0.1051 1	0.1068 1	0.1086 1	0.1103 1	0.1120 1	0.1137 1	R
	u	0.0000 0	0.3552 0	0.6677 0	0.9911 0	0.1340 1	0.1719 1	0.2128 1	0.2570 1	0.3043 1	u
	v	0.0000 0	0.0000 0	0.0000 0	0.0000 0	0.0000 0	0.0000 0	0.0000 0	0.0000 0	0.0000 0	v
	p	0.2896 3	0.2890 3	0.2877 3	0.2859 3	0.2834 3	0.2801 3	0.2756 3	0.2697 3	0.2623 3	p
	ρ	0.6294 1	0.6216 1	0.6235 1	0.6217 1	0.6185 1	0.6138 1	0.6072 1	0.5983 1	0.5869 1	ρ
5	R	0.1000 1	0.1017 1	0.1034 1	0.1051 1	0.1068 1	0.1086 1	0.1103 1	0.1120 1	0.1137 1	R
	u	0.0984 1	0.4235 0	0.7420 0	0.1077 1	0.1436 1	0.1821 1	0.2232 1	0.2671 1	0.3137 1	u
	v	0.1125 1	0.8951 0	0.8474 0	0.8652 0	0.9260 0	0.1007 1	0.1098 1	0.1190 1	0.1280 1	v
	p	0.2862 3	0.2859 3	0.2849 3	0.2833 3	0.2810 3	0.2777 3	0.2733 3	0.2675 3	0.2603 3	p
	ρ	0.6246 1	0.6175 1	0.6195 1	0.6182 1	0.6155 1	0.6114 1	0.6054 1	0.5973 1	0.5869 1	ρ
10	R	0.1000 1	0.1017 1	0.1034 1	0.1051 1	0.1068 1	0.1086 1	0.1103 1	0.1120 1	0.1137 1	R
	u	0.3579 0	0.6333 0	0.9696 0	0.1339 1	0.1729 1	0.2133 1	0.2548 1	0.2976 1	0.3419 1	u
	v	0.2030 1	0.1696 1	0.1720 1	0.1823 1	0.1949 1	0.2073 1	0.2186 1	0.2286 1	0.2372 1	v
	p	0.2770 3	0.2771 3	0.2764 3	0.2751 3	0.2731 3	0.2702 3	0.2664 3	0.2614 3	0.2553 3	p
	ρ	0.6102 1	0.6051 1	0.6078 1	0.6078 1	0.6066 1	0.6041 1	0.6002 1	0.5944 1	0.5866 1	ρ
15	R	0.1000 1	0.1017 1	0.1035 1	0.1052 1	0.1070 1	0.1087 1	0.1105 1	0.1122 1	0.1139 1	R
	u	0.7531 0	0.1011 1	0.1388 1	0.1778 1	0.2190 1	0.2591 1	0.2995 1	0.3408 1	0.3834 1	u
	v	0.2811 1	0.2523 1	0.2646 1	0.2802 1	0.2941 1	0.3060 1	0.3165 1	0.3260 1	0.3348 1	v
	p	0.2643 3	0.2648 3	0.2647 3	0.2639 3	0.2624 3	0.2602 3	0.2571 3	0.2531 3	0.2479 3	p
	ρ	0.5901 1	0.5875 1	0.5920 1	0.5944 1	0.5955 1	0.5954 1	0.5940 1	0.5910 1	0.5862 1	ρ
20	R	0.1000 1	0.1018 1	0.1036 1	0.1054 1	0.1071 1	0.1089 1	0.1107 1	0.1125 1	0.1143 1	R
	u	0.1286 1	0.1550 1	0.1965 1	0.2372 1	0.2765 1	0.3155 1	0.3548 1	0.3953 1	0.4374 1	u
	v	0.3535 1	0.3326 1	0.3509 1	0.3665 1	0.3791 1	0.3903 1	0.4012 1	0.4124 1	0.4238 1	v
	p	0.2479 3	0.2489 3	0.2494 3	0.2493 3	0.2486 3	0.2472 3	0.2452 3	0.2422 3	0.2383 3	p
	ρ	0.5638 1	0.5640 1	0.5712 1	0.5763 1	0.5802 1	0.5831 1	0.5851 1	0.5860 1	0.5857 1	ρ
25	R	0.1000 1	0.1019 1	0.1037 1	0.1056 1	0.1074 1	0.1093 1	0.1112 1	0.1130 1	0.1149 1	R
	u	0.1960 1	0.2241 1	0.2672 1	0.3065 1	0.3444 1	0.3824 1	0.4211 1	0.4612 1	0.5028 1	u
	v	0.4203 1	0.4078 1	0.4272 1	0.4405 1	0.4520 1	0.4638 1	0.4764 1	0.4897 1	0.5035 1	v
	p	0.2278 3	0.2295 3	0.2307 3	0.2315 3	0.2318 3	0.2316 3	0.2307 3	0.2292 3	0.2267 3	p
	ρ	0.5307 1	0.5346 1	0.5449 1	0.5529 1	0.5602 1	0.5670 1	0.5736 1	0.5796 1	0.5850 1	ρ
30	R	0.1000 1	0.1019 1	0.1039 1	0.1058 1	0.1078 1	0.1097 1	0.1117 1	0.1136 1	0.1156 1	R
	u	0.2763 1	0.3054 1	0.3477 1	0.3848 1	0.4213 1	0.4585 1	0.4968 1	0.5365 1	0.5778 1	u
	v	0.4785 1	0.4715 1	0.4890 1	0.5002 1	0.5117 1	0.5249 1	0.5395 1	0.5556 1	0.5725 1	v
	p	0.2048 3	0.2072 3	0.2094 3	0.2112 3	0.2126 3	0.2136 3	0.2141 3	0.2141 3	0.2134 3	p
	ρ	0.4918 1	0.4996 1	0.5129 1	0.5242 1	0.5353 1	0.5469 1	0.5589 1	0.5713 1	0.5840 1	ρ
35	R	0.1000 1	0.1021 1	0.1042 1	0.1062 1	0.1083 1	0.1104 1	0.1125 1	0.1145 1	0.1166 1	R
	u	0.3676 1	0.3965 1	0.4363 1	0.4709 1	0.5059 1	0.5421 1	0.5795 1	0.6184 1	0.6590 1	u
	v	0.5250 1	0.5217 1	0.5364 1	0.5465 1	0.5589 1	0.5737 1	0.5905 1	0.6091 1	0.6288 1	v
	p	0.1800 3	0.1833 3	0.1865 3	0.1894 3	0.1920 3	0.1942 3	0.1962 3	0.1979 3	0.1990 3	p
	ρ	0.4484 1	0.4604 1	0.4765 1	0.4914 1	0.5070 1	0.5237 1	0.5418 1	0.5616 1	0.5829 1	ρ
40	R	0.1000 1	0.1022 1	0.1044 1	0.1067 1	0.1089 1	0.1111 1	0.1133 1	0.1156 1	0.1178 1	R
	u	0.4671 1	0.4590 1	0.5306 1	0.5622 1	0.5952 1	0.6297 1	0.6658 1	0.7036 1	0.7437 1	u
	v	0.5570 1	0.5572 1	0.5693 1	0.5792 1	0.5927 1	0.6090 1	0.6279 1	0.6492 1	0.6723 1	v
	p	0.1549 3	0.1591 3	0.1633 3	0.1671 3	0.1707 3	0.1742 3	0.1776 3	0.1809 3	0.1840 3	p
	ρ	0.4029 1	0.4182 1	0.4371 1	0.4554 1	0.4753 1	0.4972 1	0.5217 1	0.5498 1	0.5816 1	ρ
45	R	0.1000 1	0.1024 1	0.1048 1	0.1073 1	0.1097 1	0.1121 1	0.1145 1	0.1169 1	0.1193 1	R
	u	0.5708 1	0.5945 1	0.6259 1	0.6546 1	0.6855 1	0.7183 1	0.7534 1	0.7907 1	0.8301 1	u
	v	0.5711 1	0.5735 1	0.5855 1	0.5970 1	0.6124 1	0.6308 1	0.6523 1	0.6770 1	0.7035 1	v
	p	0.1314 3	0.1362 3	0.1409 3	0.1454 3	0.1499 3	0.1544 3	0.1590 3	0.1638 3	0.1686 3	p
	ρ	0.3583 1	0.3759 1	0.3967 1	0.4180 1	0.4416 1	0.4684 1	0.4995 1	0.5366 1	0.5800 1	ρ

Contour plots of gasdynamic and chemistry variables are shown in Fig. 3. The results correspond to the freestream conditions of Mach number of 20 and entry altitude of 50 km. These plots are useful for conveniently analyzing the large amount of data obtained and comparing the flow phenomena. Density contours (see Ref. 20) show the density decreases rapidly along the surface of the body, while it is almost constant along the shock surface. The density gradients along the normal to the body, near the surface, are large in the supersonic region but small in the subsonic region. From the O_2 mole fraction contours,[20] one may notice the increase in concentration levels of O_2 as the flow expands around the body, causing the pressure and temperature to drop appreciably from the normal shock values and thus causing the $O-O_2$ equilibrium to shift in favor of O_2.

In Ref. 7, the gasdynamic variables for flow over a sphere of an ideal gas ($\gamma = 1.4$) are tabulated for Mach numbers 10 and 20. For future reference purposes, Table 3 is prepared in the same format as in Ref. 7, but for a Mach number of 15. The normalized radial distance from the spherical center R, r/R_N, the normalized axial and velocity componets u/v^* and v/v^*, normalized pressure p/p_∞, and normalized density ρ/ρ_∞ are tabulated as a function of normalized distance from the wall y/δ and streamwise angle θ. Table 3 will complement the already existing tables found in Ref. 7.

Conclusions

A general equilibrium chemistry, implicit finite difference computer program has been developed to solve compressible unsteady, inviscid three-dimensional flow. Equilibrium air thermodynamic properties are evaluated at each computational grid point utilizing an equilibrium composition method rather than a table look-up scheme often employed by previous investigators. The computer code has been validated through detailed comparisons with the tabulated data of Lyubimov and Rusanov for zero angle of attack. Results are obtained for Mach numbers of 10, 15, and 20 at entry altitudes of 20 and 50 km. Based on the results, it is concluded that real-gas effects are important for Mach numbers greater than 10.

Acknowledgments

The authors wish to acknowledge the helpful discussions with Dr. Paul Kutler, particularly on the shock-fitting approach. Special thanks are due to Mr. Michael J. Green for his thorough review and constructive criticism of this paper.

References

[1]Briley, W.R. and McDonald, H., "Solution of the Multidimensional Compressible Navier-Stokes Equations by a Generalized Implicit Method," *Journal of Computational Physics,* Vol. 24, 1977, pp. 372-397.

[2]Beam, R.M. and Warming, R.F., "An Implicit Factored Scheme for the Compressible Navier-Stokes Equations," *AIAA Journal,* Vol. 16, April 1978.

[3]Howe, J.T., "Introductory Aerothermodynamic of Advanced Space Transportation Systems," *Journal of Spacecraft and Rockets,* Vol. 22, Jan.-Feb. 1985, pp. 19-26.

[4]Park, C., "Radiation Enhancement by Nonequilibrium in Earth's Atmosphere," *Journal of Spacecrafts and Rockets,* Vol. 22, Jan.-Feb. 1985, pp. 27-36.

[5]Kutler, P., Pedelty, J.A., and Pulliam, T.H., "Supersonic Flow Over Three-Dimensional Ablated Nosetips Using an Implicit Numerical Procedure," AIAA Paper 80-0063, 1980.

[6]Davy, W.C., Lombard, C.K., and Green, M.J., "Forebody and Base Region Real Gas Flow in Severe Planetary Entry by a Factored Implicit Numerical Method—Part II: Equilibrium Reactive Gas," AIAA Paper 81-0282, 1981.

[7]Lyubimov, A.N. and Rusanov, V.V., "Gas Flows Past Blunt Bodies, Part II: Tables of the Gas-Dynamic Functions," NASA TT F-715, Feb. 1973.

[8]Lomax, H. and Inouye, M., "Numerical Analysis of Flow Properties About Blunt Bodies Moving at Supersonic Speeds in an Equilibrium Gas," NASA TR R-204, July 1964.

[9]Lyubimov, A.N. and Rusanov, V.V., "Gas Flows Past Blunt Bodies, Part I: Calculation Method and Flow Analysis," NASA TT F-714, Feb. 1973.

[10]Kutler, P., Reinhardt, W.A., and Warming, R.F., "Multishocked, Three-Dimensional Supersonic Flowfields with Real Gas Effects," *AIAA Journal,* Vol. 11, April 1973, pp. 657-664.

[11]Marconi, F., Salas, M., and Yaeger, L.S., "Development of a Computer Code for Calculating the Steady Super/Hypersonic Inviscid Flow Around Real Configurations," NASA CR-2675, April 1976.

[12]Li, C.P., "Numerical Simulation of Reentry Flow Around the Shuttle Orbiter Including Real gas Effects," Paper presented at ASME/AIAA Symposium on Computers in Flow Predictions and Fluid Dynamics Experiments," ASME Winter Annual Meeting, Washington, D.C., 1981.

[13]Tannehill, J.V. and Mugge, P.H., "Improved Curve Fits for the Thermodynamic Properties of Equilibrium Air Suitable for Numerical Computation Using Time-Dependent or Shock-Capturing Methods," Iowa State University, Ames, Final Report ISU-ERI-Ames-74050, Feb. 1974.

[14]Thareja, R., Szema, K.Y., and Lewis, C.H., "Viscous Shock-Layer Predictions for Hypersonic Laminar or Turbulent Flows in Chemical Equilibrium Over the Windward Surface of a Shuttle-like Vehicle," AIAA Paper 82-0201, 1982.

[15]Thareja, R., Szema, K.Y., and Lewis, C.H., "Effects of Chemical Equilibrium on Three-Dimensional Viscous Shock-Layer Analysis of Hypersonic Laminar or Turbulent Flows," AIAA Paper 82-0305, 1982.

[16]Maus, J.R., Griffith, B.J., Szema, K.Y., and Best, J.T., "Hypersonic Mach Number and Real Gas Effects on Space Shuttle Orbiter Aerodynamics," *Journal of Spacecraft and Rockets,* Vol. 21, March-April 1984, pp. 136-141.

[17]Gordon, S. and McBride, B.J., "Computer Program for Calculation of Complex Chemical Equilibrium Compositions, Rocket Performance, Incident and Reflected Shocks, and Chapman-Jouguet Detonations" NASA SP-273, 1971.

[18]Pulliam, T.H. and Steger, J.L., "On Implicit Finite-Difference Simulations of Three-Dimensional Flows," *AIAA Journal,* Vol. 18, Feb. 1980, pp. 159-167.

[19]Stull, D.R. and Prophet, H., "JANAF Thermochemical Tables," 2nd ed., NSRDS-NBS27, June 1971 (also see updates to that version supplied by Dow Chemical Co., Wilmington, Delaware).

[20]Balakrishnan, A., Davy, W.C., and Lombard, C.K., "Real Gas Flowfields About Three Dimensional Configurations," AIAA Paper 83-0581, 1983.